JOURNAL OF COMPUTATIONAL PHYSICS **145,** 671–692 (1998)
ARTICLE NO. CP986050

Truncation Error Analysis of the Rotational Form for the Convective Terms in the Navier–Stokes Equation

Kiyosi Horiuti[1] and Takao Itami

Department of Mechano-Aerospace Engineering, Tokyo Institute of Technology, 2-12-1 O-okayama, Meguro-ku, Tokyo 152, Japan
E-mail: khoriuti@mes.titech.ac.jp

Received October 7, 1997; revised April 30, 1998

The truncation error of the rotational form for the convective terms in the Navier–Stokes equation is examined in the direct numerical simulation (DNS) of the fully developed turbulent channel flow, in which the low-order finite difference method was used for the partial derivatives in the wall-normal direction. An estimate of the truncation error using the Taylor expansion revealed that this truncation error term is comparable to the rotational stress generation term, represented by the nonlinear $k-\epsilon$ model in the Reynolds averaged turbulence models, in the governing equations for the Reynolds shear stress and the normal stress due to the Coriolis force term acting in a channel flow rotating about the spanwise axis. The effective angular velocity due to the truncation error term was dependent on the distance from the wall, and the turbulence was reduced on both sides of the walls analogously to the laminarization of turbulence on the suction side of the conventional rotating channel flow. This analogy was further assessed in the DNS of the channel flow rotating with this effective angular velocity. The time development of the wall friction velocity was similar to that obtained using the rotational form.

Key Words: truncation error; rotational form; channel flow; rotation; Coriolis force; nonlinear $k-\epsilon$ model.

1. INTRODUCTION

The Navier–Stokes and continuity equations which describe the motion of incompressible fluid as

$$\frac{\partial u_i}{\partial t}+u_j\frac{\partial u_i}{\partial x_j}=-\frac{\partial p}{\partial x_i}+\frac{1}{\mathrm{Re}}\frac{\partial^2 u_i}{\partial x_k\partial x_k}+f_i, \tag{1}$$

[1] Corresponding author.

0021-9991/98 $25.00

$$\frac{\partial u_i}{\partial x_i} = 0 \tag{2}$$

are derived via the conservation laws of mass and momentum within the small fluid volumes, where Re is the Reynolds number and f_i denotes the external forces acting on the flow. When the Navier–Stokes equation is numerically discretized, it is known that, unless the (discretized) momentum and the kinetic energy are globally conserved, the result of the numerical simulation can give rise to instabilities [1]; i.e., the conservative property of the Navier-Stokes equation should be retained in the numerically discretized scheme.

The representative formulation for the convective terms in Eq. (1) which conserves the momentum and the kinetic energy is the skew-symmetric form [2, 3]

$$\frac{1}{2}\left\{ \frac{\partial}{\partial x_j}(u_i u_j) + u_j \frac{\partial u_i}{\partial x_j} \right\}, \tag{3}$$

and the rotational form [4, 5]

$$u_j \left(\frac{\partial u_i}{\partial x_j} - \frac{\partial u_j}{\partial x_i} \right) + \frac{1}{2}\frac{\partial}{\partial x_i}(u_j u_j). \tag{4}$$

Moin and Kim [6] conducted a large-eddy simulation (LES) of a fully developed turbulent channel flow using the rotational form. The pseudospectral Fourier method was used in the homogeneous directions, while the first-order finite difference method was used in the wall normal direction to approximate the partial derivatives in Eq. (4).

Horiuti [7] conducted LES of the same flow using the rotational and skew-symmetric forms. A gradual decay of the turbulent state was found when the rotational form was used, whereas good results were obtained when the skew-symmetric form was used. The poor performance of the rotational form was considered to be attributable to its large truncation errors in the vicinity of the wall arising in the first-order finite difference method.

Zang [8] reported extensive numerical experiments on the comparison of these two formulations in various turbulent flows using the spectral method. He demonstrated that the skew-symmetric form gives fairly good results even in the presence of aliasing errors, whereas the rotational form performed poorly. The destabilizing effect of the aliasing errors in the rotational form was recognized in the wiggles of the contour plots, illustrating the vorticity distributions, but the decay of turbulence observed in [7] was not reported.

Blaisdell *et al.* [9] presented a theoretical explanation as to why aliasing errors are reduced for the skew-symmetric form. Kravchenko and Moin [10] compared various formulations for the convective terms in LES of turbulent channel flow, in which the effect of the dealiasing for the convective terms was examined. They found that the difference between the results of the aliased and dealiased simulations was large for the rotational form, whereas it was minimal for the skew-symmetric form, confirming the results of Zang [8].

All these results consistently showed that the skew-symmetric form is superior to the rotational form, but there are two important errors arising in the convective terms: one is the aliasing error and the other is the truncation error. In reality, these two issues are not separable. For example, in [10], it was pointed out that the aliasing error is the leading source of error for the spectral method, while the truncation error is the leading source for the low-order finite difference method.

Although the role of the aliasing error has been clearly revealed, as yet no physical significance of the truncation error has been clearly shown. The purpose of the present

work is to investigate the mechanism of turbulence decay observed in [7] by examining the role of the truncation error.

The previous analysis in [7] was carried out in LES of turbulent channel flow. It is felt that the poor performance of the rotational form may be attributable to the interference of the turbulence model employed in LES to approximate the subgrid-scale correlations with the numerical scheme used in the simulation. To eliminate the effect arising in this interference, we carry out the present analysis in the framework of the direct numerical simulation (DNS) of a fully developed turbulent channel flow without turning to the subgrid-scale models, in which the aliasing errors were eliminated.

The numerical methods used in the present study are briefly described in Section 2, while Section 3 presents the numerical results. In Section 4, the analysis of the truncation error for the rotational form is presented, and its significance is interpreted in relation to the channel flow with rotation. A numerical scheme which eliminates the drawback of the rotational form is presented in Section 5. Our conclusions are given in Section 6.

2. NUMERICAL METHOD

The numerical method used in the present paper is identical to that used by Horiuti [7], except for the dealiasing for the convective terms. Dealiasing was implemented by expanding the number of collocation points by a factor of $\frac{3}{2}$ before transformation into the physical space ($\frac{3}{2}$-rule) [4].

The indices $i = 1, 2, 3$ in Eqs. (1) and (2) correspond to the directions x, y, and z, respectively, where x is the streamwise direction, y is the wall-normal direction, and z is the spanwise direction. For notational simplicity, the velocity components (u_1, u_2, u_3) are occasionally denoted by (u, v, w). Grid points in the y direction are located at the Chebyshev–Gauss–Lobatto quadrature points [4] as

$$\frac{y_j}{\delta} = -\cos\left(\frac{\pi j}{N}\right), \tag{5}$$

where y_j is the coordinate of the jth grid point in the y direction, and δ is the half-channel height, and N is the number of grid points in the y direction.

We assume that fields are homogeneous in two directions (x and z), and impose the periodic boundary conditions in these two directions, while the no-slip boundary condition on the two walls is imposed in the y direction. The pseudospectral Fourier expansion method was used in the x and z directions, whereas the central finite difference method was used in the y direction. In the following, $\langle f \rangle$ denotes a running time average of the instantaneous horizontal $(x - z)$ plane average of f, and f' denotes the deviation of f from the plane average of f.

For discretizing Eq. (1) in time, the convective and pressure-gradient terms were approximated by the second-order Adams–Bashforth scheme while the Crank–Nicolson scheme was used for the viscous terms.

The two formulations of the convective terms were compared in the DNS of a fully developed channel flow with Re_τ (Reynolds number based on the wall-friction velocity, u_τ, and δ) = 180; 128, 129, and 128 grid points were used, respectively, in the x, y, and z directions. In the following the subscript + denotes a nondimensional quantity scaled by the wall variable u_τ and the kinematic viscosity ν. The flow was driven by the mean pressure gradient imposed in the downstream direction.

A regular mesh system is adopted, and all velocity components and pressure are defined at grid points y_j, as given by Eq. (5), and both the momentum and continuity equations were enforced at these grid points.

Two approximation schemes were used for the first-order partial differential operators in the y direction. One is the first-order central finite differences

$$\left(\frac{\partial u}{\partial y}\right)_{i,j,k} \sim \left(\frac{\delta u}{\delta y}\right)_{i,j,k} = \frac{u_{i,j+1,k} - u_{i,j-1,k}}{h_{j+1} + h_j}, \tag{6}$$

where $(f)_{i,j,k}$ and $f_{i,j,k}$ denote the values of f at the grid point (x_i, y_j, z_k) $(x_i = i\Delta x$, $z_k = k\Delta z)$, and $h_j = y_j - y_{j-1}$. Δx and Δz are the grid intervals in the x and z directions, respectively. $\delta/\delta y$ denotes the finite-difference approximation of the partial derivative $\partial/\partial y$. The other is the second-order central finite differences

$$\left(\frac{\partial u}{\partial y}\right)_{i,j,k} \sim \left(\frac{\delta u}{\delta y}\right)_{i,j,k} = \frac{h_j}{(h_{j+1} + h_j)h_j} u_{i,j+1,k} + \frac{(h_{j+1} - h_j)}{h_{j+1}h_j} u_{i,j,k} - \frac{h_{j+1}}{(h_{j+1} + h_j)h_{j+1}} u_{i,j-1,k}. \tag{7}$$

Second-order partial differential operators in the y direction were approximated with the second-order central finite differences as

$$\left(\frac{\partial^2 u}{\partial y^2}\right)_{i,j,k} \sim 2\left(\frac{u_{i,j-1,k}}{(h_{j+1} + h_j)h_j} - \frac{u_{i,j,k}}{h_{j+1}h_j} + \frac{u_{i,j+1,k}}{(h_{j+1} + h_j)h_{j+1}}\right). \tag{8}$$

3. NUMERICAL RESULTS

The initial values used in the computations were those obtained by DNS using the Fourier–Chebyshev polynomials expansion method with $\mathrm{Re}_\tau = 180$, with 128, 129, and 128 grid points, respectively, in the x, y, and z directions [11], in which aliasing errors were removed using the 3/2-rule. The size of the computational domain in the x and z directions were $L_x = 6.4\delta$ and $L_z = 3.2\delta$, respectively. The time increment was chosen to be 0.0002. In all the computed cases shown in the following, the same Reynolds number, grid points, and computational domain size were used. When the computational results reached statistical equilibrium, the first- and second-order partial differential operators in the y-direction were switched to finite differences, i.e., Eq. (7) for the first-order operators and Eq. (8) for the second-order operators. The convective terms were approximated using the skew-symmetric form. The computation was further carried out until it reached equilibrium (approximately for 10 nondimensional time units (δ/u_τ)). Time averages were calculated for approximately six time units, after the computation reached equilibrium (Case I).

In good agreement with the result reported by Horiuti [7], the turbulence state was sustained using the skew-symmetric form for the convective terms. We compare the computed results with those obtained using the Fourier–Chebyshev polynomial expansion method [12]. In [12], 192, 129, and 160 grid points were used, respectively, in the x, y, and z directions. The size of the computational domain in the x and z directions were $4\pi\delta$ and $2\pi\delta$, respectively. In the present study, smaller numbers of grid points were used. To provide a sufficient grid resolution, we have chosen a smaller size of the computational domain in these two directions. We note that both streamwise and spanwise length of the computational domain ($L_{x+} = 1152$, $L_{z+} = 576$, respectively) are much larger than the minimum size of the

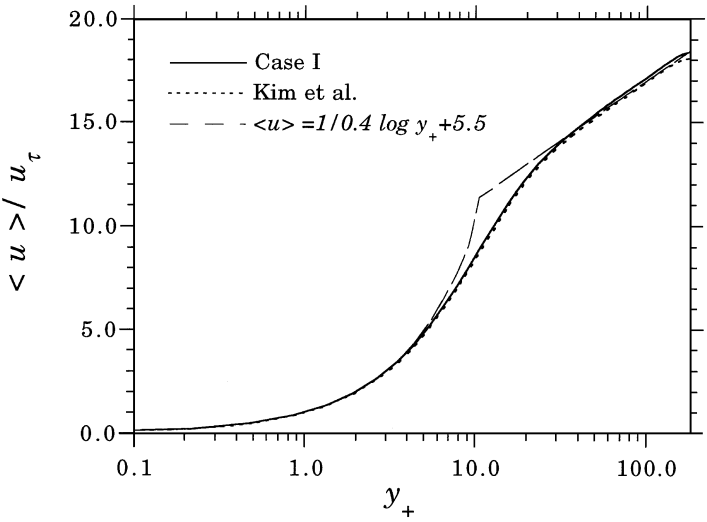

FIG. 1. Mean streamwise velocity profiles obtained for Case I and by Kim *et al.* [13].

periodic computational box that would sustain turbulence ($L_{x+} \approx 250 - 350$, $L_{z+} \approx 100$) (the minimal flow unit [13]).

Figure 1 shows the mean velocity profiles obtained in Case I and by Kim *et al.* [12]. The present results lie slightly above the data of Kim *et al.* [12]. Nishioka *et al.* [14] showed that Clauser's parameter G $(=(U_C/u_\tau)(H-1)/H$, where H denotes the shape factor and U_C is the centerline velocity) can be used as an indicator to determine whether the computed mean velocity profile predicts the logarithmic law profile. They found that when $G \leq 7.0$, the mean velocity obeys the logarithmic law and that otherwise it does not. The G values were 7.02 and 7.06, respectively, for the results obtained by Kim *et al.* [12] and in Case I. In both sets of results, the values of G are close to 7.0, although the present value is slightly larger than that reported by Kim *et al.* [12].

The von Kármán constant obtained in Case I was ≈0.38, which is slightly smaller than the experimentally determined value of 0.4 [14], whereas that in [12] was approximately equal to 0.4. The intercept of the logarithmic law profile (constant B) for the present result (≈5.0) is smaller than that obtained from [12] (≈5.5).

The profiles of the turbulence intensities are shown in Fig. 2. In the present results, the peak value of the streamwise component is a slight overestimate of that in [12], whereas both the wall-normal and spanwise components are slightly underestimated.

The distributions of the Reynolds shear stress are shown in Fig. 3. The straightline profile of the total shear stress, $\langle u'v' \rangle - (1/\mathrm{Re})\partial\langle u \rangle/\partial y$, indicates that the stress is balanced by the mean pressure gradient and the flow is in an equilibrium state. The amplitude of $\langle u'v' \rangle$ obtained in Case I is slightly larger than that in [12].

Two reasons for a decreased performance accuracy of the results from Case I, compared with the results obtained by Kim *et al.* [12], can be considered. The principal reason may be the difference in the method of approximating the partial differential operator $\partial/\partial y$. Kravchenko and Moin [10] reported a shifting up of the mean velocity profile and the overestimation of the streamwise turbulence intensity when the second-order finite difference method is used, which is in good agreement with the present result. Another reason may be the difference in the size of the computational domain, although the wall region is rather

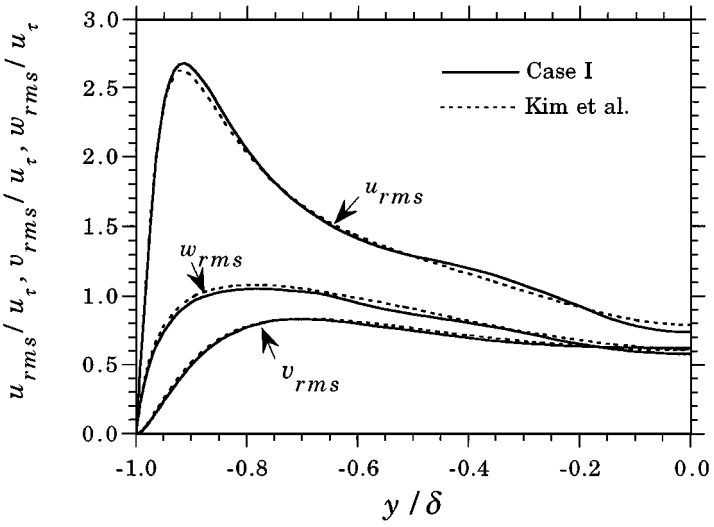

FIG. 2. y-distributions of turbulence intensities obtained for Case I and by Kim *et al.* [13]. $u_{\rm rms}$ denotes root-mean-square value of u.

well resolved in the present study with $\Delta x_+ = 9.0$ and $\Delta z_+ = 4.5$, while $\Delta x_+ \approx 11.8$ and $\Delta z_+ \approx 7.0$ in [12].

Using the presented data as the initial values, we investigated the difference in the results obtained using different formulations for the convective terms.

In Case II, the rotational form was used throughout the channel ($-\delta \le y \le \delta$). The computed cases are summarized in Table I.

In Fig. 4, the temporal variations of the wall friction velocities, u_τ, at the lower wall obtained for Case I and Case II, normalized by the initial value of the wall friction velocity, $u_{\tau 0}$, are shown. Similar results were obtained at the upper wall (figure not shown); u_τ gradually decreased in Case II, while u_τ remained close to unity in Case I, as was previously

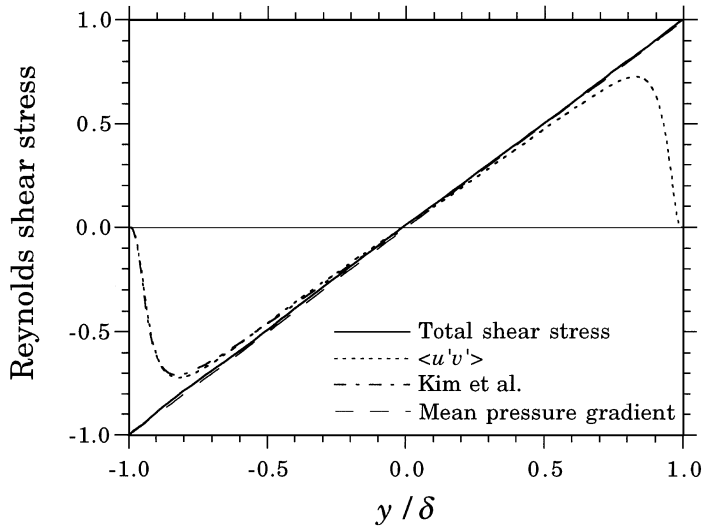

FIG. 3. y-distributions of the Reynolds shear stress obtained for Case I and by Kim *et al.* [12].

TABLE I
Case Specifications, Formulations of Approximation for the Convective Terms, and the Coriolis Force Term

Case	Convective terms	Coriolis force term
I	Skew-symmetric ($-1 \le y/\delta \le 1$)	None
II	Rotational ($-1 \le y/\delta \le 1$)	Error term
III	Skew-symmetric ($-1 \le y/\delta \le 1$)	Eq. (27)

found in [7]. The turbulent state gradually decayed when the rotational form was used, while it was sustained when the skew-symmetric form was used.

Figure 5 shows the profiles of the Reynolds shear stress normalized by $u_{\tau 0}$ obtained for Case II at $t\,u_{\tau 0}/\delta = 5.0$. In good agreement with the wall friction velocity shown in Fig. 4, the total stress at both walls is ≈ 0.7, implying that the turbulence is substantially reduced.

The profiles of the normal component of the turbulence intensity, $\langle v'v' \rangle^{1/2}$, at $t\,u_{\tau 0}/\delta = 5.0$ for Case I and Case II are shown in Fig. 6. The intensity obtained for Case II is smaller than that for Case I and the peaks of the intensity found in the result for Case I are indiscernible in the result obtained for Case II, indicating that the turbulence is decaying in time in Case II. The streamwise and spanwise components of intensities showed similar results, but the decrease of the normal component was the maximum.

Figure 7 shows the budget of the turbulent shear stress, $\langle u'v' \rangle$, in the vicinity of the lower wall, nondimensionalized with $u_{\tau 0}^4/\nu$ obtained for Case I and Case II. The governing equation for $\langle u'v' \rangle$ is expressed as

$$\frac{\partial \langle u'v' \rangle}{\partial t} = -\langle v'v' \rangle \frac{\partial \langle u \rangle}{\partial y} - \frac{\partial \langle u'v'v' \rangle}{\partial y} - \left\langle u' \frac{\partial p}{\partial y} + v' \frac{\partial p}{\partial x} \right\rangle + \frac{1}{\mathrm{Re}_\tau} \frac{\partial^2 \langle u'v' \rangle}{\partial y \partial y} - 2 \frac{1}{\mathrm{Re}_\tau} \left\langle \frac{\partial u'}{\partial x_j} \frac{\partial v'}{\partial x_j} \right\rangle. \tag{9}$$

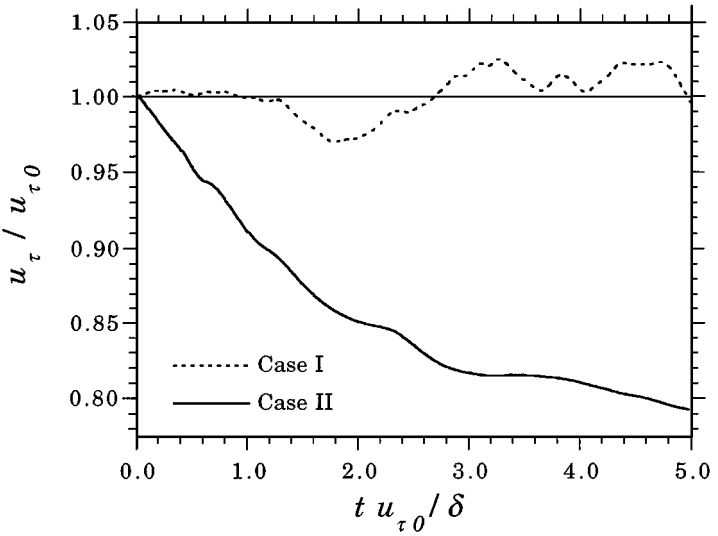

FIG. 4. Time evolution of the wall friction velocity, u_τ, at the lower wall obtained for Case I and Case II.

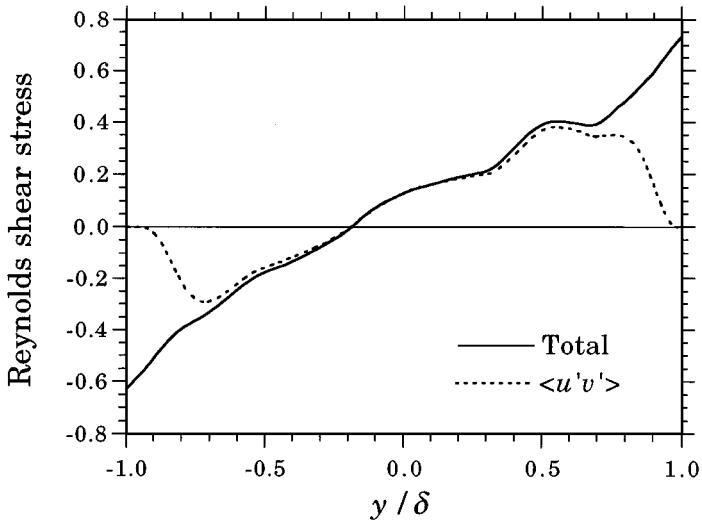

FIG. 5. y-distributions of the Reynolds shear stress obtained for Case II.

The terms on the right-hand side of Eq. (9) are called the production, convection, velocity–pressure gradient, diffusion, and dissipation terms, respectively. Note that the distributions of the diffusion and dissipation terms are not included in Fig. 7 because their amplitude was small.

Figures 7a and b show the distributions near the lower wall for Case II and Case I, respectively. Note that the Reynolds shear stress has a negative sign in the lower half of the channel. A marked difference is seen in the results obtained using the rotational and the skew-symmetric forms. The velocity–pressure gradient term obtained using the rotational form shows a large negative peak at $y_+ \sim 10$ and becomes positive away from the wall, whereas that obtained using the skew-symmetric form remains positive.

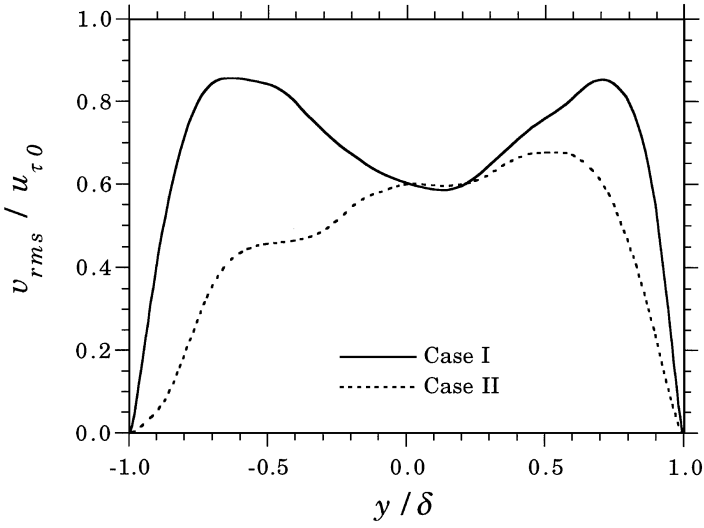

FIG. 6. y-profiles of the normal component of the turbulence intensity, $\langle v'v' \rangle^{1/2}$, at $t\, u_{\tau 0}/\delta = 5.0$ for Case I and Case II.

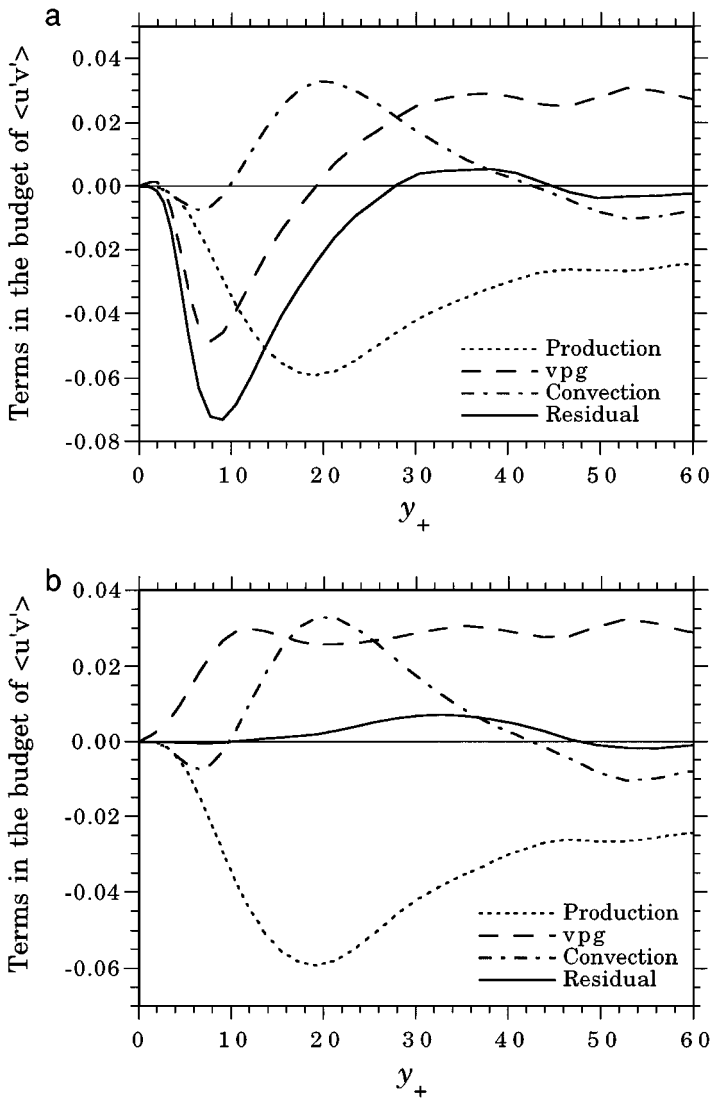

FIG. 7. Balance of the turbulent shear stress, $\langle u'v' \rangle$: (a) Case II; (b) Case I. (vpg denotes the velocity–pressure gradient term.)

It is observed that the residual of the terms in the budget of Eq. (9) shown in Fig. 7b is very small, whereas the residual is a large negative value near the lower wall for the budget shown in Fig. 7a. This imbalance found in Fig. 7a is inconsistent with the decay of turbulence observed in Fig. 4, because the negative residual indicates that $\partial \langle u'v' \rangle / \partial t < 0$. This negativity implies that $\langle u'v' \rangle$ becomes a much larger negative value with the lapse of time. In turn, it implies an increase of the streamwise component of turbulence intensity via the shear production term, $-\langle u'v' \rangle (\partial \langle u \rangle / \partial y)$, in the lower half of the channel. This inconsistency will be discussed in the following section.

A notable difference was also found in the budget of the normal component of the turbulent energy $\langle v'v' \rangle$ (figure not shown) between the results obtained using the skew-symmetric form and the rotational form, as pointed out by Horiuti [7]. The DNS results obtained using

the Fourier–Chebyshev polynomial expansion method shown in [12] and [15] are similar to the results obtained using the skew-symmetric form.

The present results are in good agreement with the results obtained using the LES method reported by Horiuti [7]. It is shown that the laminarization of the turbulent state observed in [7] is not intrinsic to the turbulence model employed in LES, but is intrinsic to the formulation of the approximation method for the convective terms in the Navier–Stokes equation.

4. ANALYSIS OF TRUNCATION ERRORS

In this section, we conduct the analysis of the truncation error for the rotational form. In [7], it was pointed out that the major error in the rotational form comes from the truncation of the term

$$-u\frac{\delta u}{\delta y}+\frac{1}{2}\frac{\delta u^2}{\delta y}, \tag{10}$$

contained in the y-momentum equation, whereas no serious error is introduced using the skew-symmetric form when the low-order finite difference method is used. These points were confirmed in the present study.

4.1. *Estimate of Truncation Errors Involved in the Rotational Form*

When the first-order partial differential operators in Eq. (10) are approximated by the first-order central finite differences (Eq. (6)), we obtain an estimate of the exact truncation error term, Eq. (10), using the Taylor expansion, as

$$\frac{h_{j+1}-h_j}{2}\left(\frac{\partial u}{\partial y}\right)_j^2+\frac{h_{j+1}^2-h_{j+1}h_j+h_j^2}{4}\left\{\frac{\partial}{\partial y}\left(\frac{\partial u}{\partial y}\right)^2\right\}_j. \tag{11}$$

The first and second terms in Eq. (11) are first and second order with respect to the grid interval h_j, respectively.

The corresponding error for the second-order finite difference, Eq. (7), is estimated as

$$\frac{h_{j+1}h_j}{4}\left\{\frac{\partial}{\partial y}\left(\frac{\partial u}{\partial y}\right)^2\right\}_j, \tag{12}$$

in which the leading term is of second order. The identical truncation error terms with different coefficients are contained in the first- (Eq. (11)) and the second- (Eq. (12)) order finite difference.

We examine the contribution of the truncation error term, Eq. (10), in the balance of the turbulent shear stress as

$$-\left\langle u'\left(-u\frac{\delta u}{\delta y}+\frac{1}{2}\frac{\delta u^2}{\delta y}\right)\right\rangle, \tag{13}$$

which is obtained by multiplying u' to the y-momentum equation. The y-distributions of the term, Eq. (13), obtained using the first-order and second-order finite difference

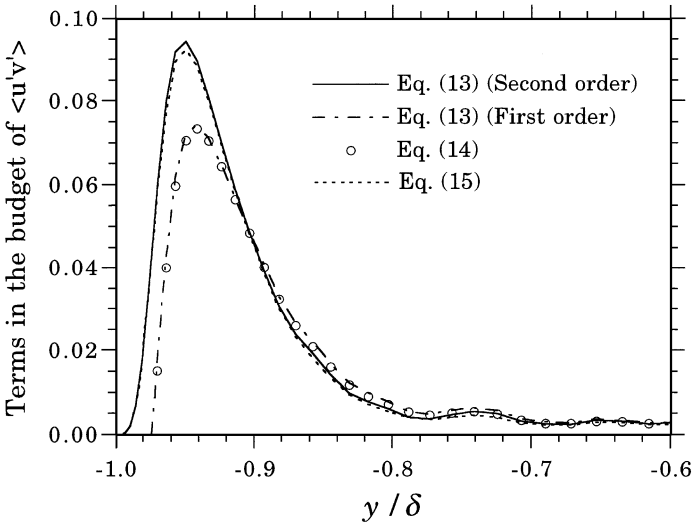

FIG. 8. y-profiles of the exact truncation error term in the balance of the turbulent shear stress, Eq. (13), and the error term approximated using the Taylor expansion, Eq. (14) and Eq. (15).

approximations for $\delta/\delta y$, are shown in Fig. 8. The term contained in Eq. (13) is computed using the velocity data obtained in Case I. The result obtained using the first-order finite difference approximation is similar to that obtained using the second-order approximation, although the peak value is smaller for the result obtained using the first-order approximation than for that obtained using the second-order approximation.

In Fig. 8, we included the distributions of the error term approximated using the Taylor expansion, Eq. (11), in the balance of the turbulent shear stress as

$$-\left\langle u'\left[\frac{h_{j+1}-h_j}{2}\left(\frac{\partial u}{\partial y}\right)_j^2+\frac{h_{j+1}^2-h_{j+1}h_j+h_j^2}{4}\left\{\frac{\partial}{\partial y}\left(\frac{\partial u}{\partial y}\right)^2\right\}_j\right]\right\rangle, \tag{14}$$

and that approximated using the Taylor expansion, Eq. (12), as

$$-\left\langle u'\frac{h_{j+1}h_j}{4}\left\{\frac{\partial}{\partial y}\left(\frac{\partial u}{\partial y}\right)^2\right\}\right\rangle. \tag{15}$$

It is observed that the distributions of Eq. (13) approximated using the first-order finite difference method for $\delta/\delta y$ and Eq. (14) are almost identical. A similar result is obtained for the second-order finite difference method, indicating that the estimate of the truncation error term obtained using the Taylor expansion is very accurate.

In [7], it was shown that the first term in Eq. (11) is proportional to Re_τ^2 in the vicinity of the wall and that it introduces a large error into the y-momentum equation. Associated with this large error, the result obtained using the first-order approximation in Fig. 8 shows a large negative value near the wall. This large error can be eliminated by inserting the velocity components, which are split into the mean streamwise velocity and its deviation part, i.e., $u_i = \langle u_i\rangle\delta_{i1} + u_i'$, into the rotational form [7]. When this splitting is inserted, however, the laminarization of the turbulent state observed in the previous section is not prevented. Thereby, the first term in Eq. (11) is not the dominant truncation error term; the

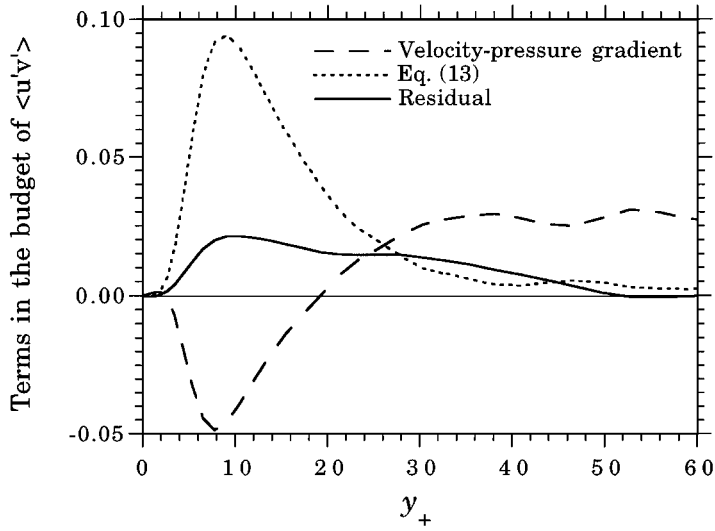

FIG. 9. y-profiles of the velocity–pressure gradient term, Eq. (13), and the residual of the terms in the budget of $\langle u'v' \rangle$, including Eq. (13).

most significant contribution arises in the second term in Eq. (11). In fact, the region with a large negative value shown in Fig. 8 is confined only to the immediate vicinity of the wall ($y/\delta \leq -0.98$).

For brevity, we carried out the following analysis using the second-order central finite differences (Eq. (7)) for the first-order partial differential operators.

We examine the contribution of the term in Eq. (13) in the budget of $\langle u'v' \rangle$ using Fig. 9, in which the distributions of the velocity–pressure gradient term, the term in Eq. (13), and the residual of the terms in the budget of $\langle u'v' \rangle$, including Eq. (13), are shown. The truncation error term, Eq. (13), is very large, even when the dense grid points of 129 for the present Reynolds number are used, and balances the velocity–pressure gradient term. It should be noted that the residual is now positive, which indicates that $\partial \langle u'v' \rangle / \partial t > 0$. This positivity implies that $\langle u'v' \rangle$ obtains a much smaller negative value with the lapse of time, which in turn, results in a suppression of the streamwise component of turbulence intensity via the reduction of the shear production term, $-\langle u'v' \rangle (\partial \langle u \rangle / \partial y)$. Thus, the inconsistency found in the budget of $\langle u'v' \rangle$ shown in Fig. 7a is eliminated.

Equation (15) can be rearranged as

$$\left\langle \frac{h_{j+1}h_j}{4} \left[-\frac{\partial}{\partial y} \left\{ u' \left(\frac{\partial u}{\partial y} \right)^2 \right\} + \frac{1}{2} \frac{\partial u'}{\partial y} \left(\frac{\partial u}{\partial y} \right)^2 \right] \right\rangle. \tag{16}$$

When the two terms in Eq. (16) are integrated with respect to y from the lower wall to the upper wall, the first term vanishes, while the second term remains, implying that the second term is a major term. The second term can be rearranged by inserting the decomposition of the velocity into the mean and the fluctuation parts, $u = \langle u \rangle + u'$, as

$$\frac{h_{j+1}h_j}{2} \frac{\partial \langle u \rangle}{\partial y} \left\langle \left(\frac{\partial u'}{\partial y} \right)^2 \right\rangle + \frac{h_{j+1}h_j}{4} \left\langle \left(\frac{\partial u'}{\partial y} \right)^3 \right\rangle. \tag{17}$$

It was found that distribution of the term $\langle (\partial u'/\partial y)^2 \rangle$ was similar to that of the term

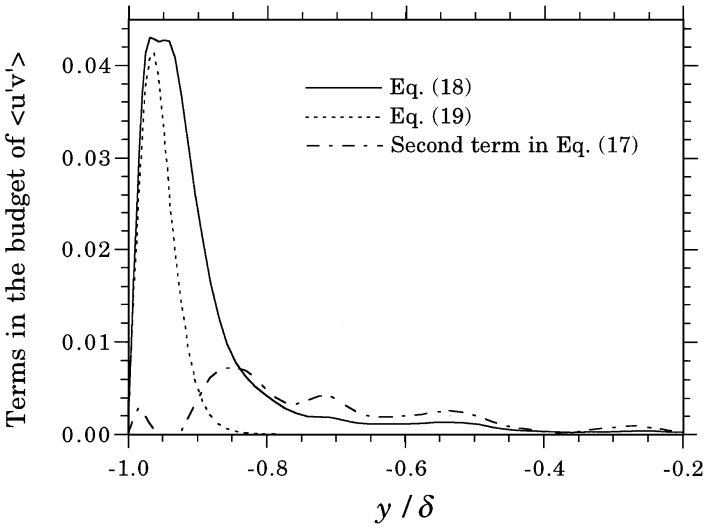

FIG. 10. y-profiles of the second term in Eq. (17), the term in Eq. (18), and the term in Eq. (19).

$(\partial\langle u\rangle/\partial y)^2$; i.e.,

$$\frac{h_{j+1}h_j}{2}\frac{\partial\langle u\rangle}{\partial y}\left\langle\left(\frac{\partial u'}{\partial y}\right)^2\right\rangle \tag{18}$$

$$\simeq C_1\frac{\partial\langle u\rangle}{\partial y}\frac{h_{j+1}h_j}{2}\left(\frac{\partial\langle u\rangle}{\partial y}\right)^2, \tag{19}$$

where C_1 is a numerical factor ($\simeq$0.4). The distributions of the terms in Eq. (18) and Eq. (19) are compared in Fig. 10. Although the term in Eq. (18) has a longer tail away from the wall than the term in Eq. (19), the two terms are generally similar. For comparison, the profile of the second term in Eq. (17) is included in Fig. 10. It can be seen that the contribution of this term is insignificant near the wall. Therefore, Eq. (16) can be approximated as

$$\left\langle\frac{h_{j+1}h_j}{4}\left[-\frac{\partial}{\partial y}\left\{u'\left(\frac{\partial u}{\partial y}\right)^2\right\}+\frac{1}{2}\frac{\partial u'}{\partial y}\left(\frac{\partial u}{\partial y}\right)^2\right]\right\rangle \simeq C_1\frac{\partial\langle u\rangle}{\partial y}\frac{h_{j+1}h_j}{2}\left(\frac{\partial\langle u\rangle}{\partial y}\right)^2. \tag{20}$$

We note that in the evaluation of Eqs. (14), (15), (17), (18), and (19), the partial derivatives $\partial/\partial y$ were approximated using the second-order finite difference, Eq. (7), so that the partial derivatives in these equations can just as well be evaluated by exact derivatives up to the leading-order terms. We have also conducted an evaluation using the Chebyshev polynomial expansions and obtained results similar to those shown in the present paper, because the leading terms were identical for these two approximation methods.

4.2. *Relationship of the Truncation Error with Nonlinear $k-\epsilon$ Model and Rotating Channel Flow*

In the previous section, it was shown that the truncation error associated with the first- and second-order finite differences yields an extra term in the budget of the turbulent shear stress, and its contribution to the budget is considerably large. The role of this extra term,

however, has not yet been clearly revealed. By turning to the nonlinear $k-\epsilon$ model for the Reynolds stresses in the Reynolds averaged turbulence models [16], we show that the role of the major truncation error term, Eq. (20), is analogous to that of the Coriolis force term in channel flow rotating about the z-axis.

The nonlinear $k-\epsilon$ model has been successfully used to express the anisotropy of the turbulence intensities in the sheared turbulence (see Speziale [16] and references therein). For flows which are homogeneous in two directions, this model yields the approximation of the Reynolds stresses as

$$\begin{aligned}
\langle u'u'\rangle &\simeq \frac{2}{3}k + \frac{k^3}{\epsilon^2}\left\{\left(\frac{2}{3}C_{\tau 1} - \frac{1}{3}C_{\tau 3}\right)\left(\frac{\partial\langle u\rangle}{\partial y}\right)^2\right\},\\
\langle v'v'\rangle &\simeq \frac{2}{3}k + \frac{k^3}{\epsilon^2}\left\{\left(-\frac{1}{3}C_{\tau 1} + \frac{2}{3}C_{\tau 3}\right)\left(\frac{\partial\langle u\rangle}{\partial y}\right)^2\right\},\\
\langle w'w'\rangle &\simeq \frac{2}{3}k + \frac{k^3}{\epsilon^2}\left\{\left(-\frac{1}{3}C_{\tau 1} - \frac{1}{3}C_{\tau 3}\right)\left(\frac{\partial\langle u\rangle}{\partial y}\right)^2\right\},
\end{aligned} \tag{21}$$

where k denotes the turbulent kinetic energy, $k=\langle u'u'+v'v'+w'w'\rangle/2$, ϵ denotes the dissipation rate of k, and $C_{\tau 1}$ and $C_{\tau 3}$ are model parameters. The values for $C_{\tau 1}$ and $C_{\tau 3}$ contained in Eq. (21) were optimized in the simulation of turbulent channel flow, where the values for k and ϵ were provided by solving the governing equations for k and ϵ using the $k-\epsilon$ model [16]. It was shown that $C_{\tau 1}$ is positive ($\simeq$0.05) and $C_{\tau 3}$ is negative ($\simeq -0.01$) [16], so that the turbulence intensities are correctly predicted as $\langle u'u'\rangle > \langle w'w'\rangle > \langle v'v'\rangle$ near the wall.

From Eq. (21), we derive the approximation for the term $\langle u'u' - v'v'\rangle$ as

$$\langle u'u' - v'v'\rangle \simeq \frac{k^3}{\epsilon^2}\left\{(C_{\tau 1} - C_{\tau 3})\left(\frac{\partial\langle u\rangle}{\partial y}\right)^2\right\}, \tag{22}$$

in which the term identical to the term in Eq. (20) is found, although their coefficients differ. In the nonlinear $k-\epsilon$ model, the length scale is represented by the term $k^{3/2}/\epsilon$ [17], whereas it is represented by the term $\sqrt{(h_{j+1}h_j)/2}$ in Eq. (20).

The present analysis shows that the truncation error term, Eq. (13), can be approximated as

$$-\left\langle u'\left(-u\frac{\delta u}{\delta y} + \frac{1}{2}\frac{\delta u^2}{\delta y}\right)\right\rangle \simeq -2\Omega_R\langle u'u' - v'v'\rangle, \tag{23}$$

$$\Omega_R = C_R\frac{\partial\langle u\rangle}{\partial y}, \tag{24}$$

by noting that the term in Eq. (20) is multiplied by the term $\partial\langle u\rangle/\partial y$, where C_R is a numerical constant. The right-hand side of Eq. (23) corresponds to the rotational stress generation term in the channel flow rotating with the effective angular velocity Ω_R about the z-axis.

In Fig. 11, the distribution of the truncation error term, Eq. (13), is shown with the rotational stress generation term $-2\Omega_R\langle u'u' - v'v'\rangle$. They are almost identical when C_R is chosen to be -0.0115, indicating that in the budget of the turbulent shear stress, the error term behaves analogously to the Coriolis force term acting in the rotating channel flow.

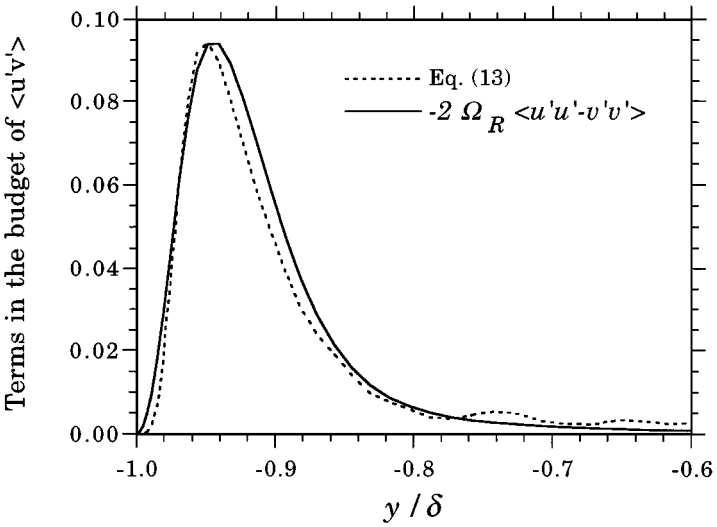

FIG. 11. y-profiles of the truncation error term in the budget of $\langle u'v' \rangle$, Eq. (13), and the rotational stress generation term $-2\Omega_R \langle u'u' - v'v' \rangle$.

The results obtained in the present paper are similar to those reported in [7] despite the difference in the numerical method (DNS in the present study and LES in [7]), the difference in the Reynolds number ($\mathrm{Re}_\tau = 180$ in the present study and 640 in [7]), and the difference in the mesh configurations. It may be considered that the agreement of the truncation error term and the Coriolis force term, Eq. (23), is a numerical coincidence, but based on the comparison of the results of these two studies and on the observation that the truncation error term can be analytically correlated to the Coriolis force term via the nonlinear $k - \epsilon$ model, we consider that this agreement is not a mere coincidence.

However, there are similarities and differences between the pure Coriolis force term and the truncation error term associated with the rotational form.

The angular velocity, Ω_R, is dependent on the distance from the wall, unlike the Coriolis force acting on the pure rotating channel in which the angular velocity, Ω, is constant throughout the channel. Because Ω is constant for pure rotating channel flow, an asymmetry of the Coriolis force acting on the velocity fields arises between the lower and upper halves of the channel [18]. When Ω is negative, the turbulence is reduced in the lower half of the channel (suction side), while it is enhanced in the upper half of the channel (pressure side).

In contrast, the sign of the effective angular velocity for the truncation error term, Ω_R, is dependent on the y coordinate. Ω_R is very large in close proximity to the walls because $\partial \langle u \rangle / \partial y \simeq \mathrm{Re}_\tau$ in these regions, but rapidly decreases with the distance from the wall. Its sign is negative in the lower half and positive in the upper half of the channel, and thus asymmetry does not arise. The dimensionless parameter, S ($=-2\Omega_R/(\partial \langle u \rangle / \partial y)$), defined in [18] is constant throughout the channel ($=0.023$). As was shown in [18], the positive S is associated with the stabilized flow, and the turbulence level is lowered in both the lower and upper halves of the channel.

Table II lists the correspondence of the terms in the budget of the Reynolds stresses between the terms due to the Coriolis force (rotational stress generation term) for the rotating channel and the truncation error terms due to the rotational form. It was found that in the budget of the normal component of turbulence fluctuations, $\langle v'v' \rangle$, there is a term

TABLE II

Correspondence between the Rotational Stress Generation Term for the Rotating Channel and the Truncation Error Term for the Rotational Form in the Budget of the Reynolds Stresses

Reynolds stress	Rotational stress generation term	Truncation error term
$\langle u'u' \rangle$	$4\Omega_R \langle u'v' \rangle$	None
$\langle v'v' \rangle$	$-4\Omega_R \langle u'v' \rangle$	$-2\left\langle v'\left(-u\frac{\partial u}{\partial y}+\frac{1}{2}\frac{\partial u^2}{\partial y}\right)\right\rangle$
$\langle u'v' \rangle$	$-2\Omega_R \langle u'u'-v'v' \rangle$	$-\left\langle u'\left(-u\frac{\partial u}{\partial y}+\frac{1}{2}\frac{\partial u^2}{\partial y}\right)\right\rangle$

corresponding to the Coriolis force term:

$$-2\left\langle v'\left(-u\frac{\delta u}{\delta y}+\frac{1}{2}\frac{\delta u^2}{\delta y}\right)\right\rangle. \tag{25}$$

Figure 12 shows the y-distributions of the term in Eq. (25), and the rotational stress generation term due to the angular velocity, Ω_R, as

$$-4\Omega_R \langle u'v' \rangle, \tag{26}$$

where C_R was set as -0.0115. They are similar to each other in the vicinity of the wall ($y/\delta = -1.0 \sim -0.95$). In this region, the direct effect of the Coriolis force term and the error term is to reduce the amplitude of $\langle v'v' \rangle$. At a distance from the wall, the truncation error term becomes positive, while the rotational stress generation term remains negative, but in this region, the contribution of the truncation error term to the budget of $\langle v'v' \rangle$ is small. Thereby, the normal fluctuation is damped, as shown in Fig. 6, due to the truncation error term.

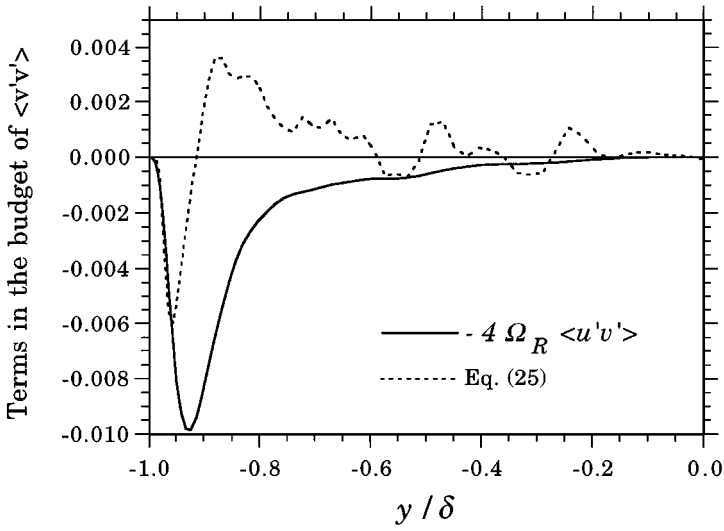

FIG. 12. y-profiles of the truncation error term in the budget of $\langle v'v' \rangle$, Eq. (25), and the rotational stress generation term $-4\Omega_R \langle u'v' \rangle$.

It should be noted that, in the budget of the streamwise component of turbulent fluctuations, $\langle u'u' \rangle$, there is no truncation error term corresponding to the rotational stress generation term because there is not significant error term in the x-momentum equation. In the system rotating with angular velocity Ω or Ω_R, the rotational stress generation terms in the budgets of $\langle u'u' \rangle$ and $\langle v'v' \rangle$ cancel each other; i.e., the turbulent kinetic energy is conserved in the presence of the Coriolis force term, while it is not conserved in the presence of the extra term due to the truncation error. However, the amplitude of the normal fluctuation, $\langle u'u' \rangle$, is reduced via a reduction of the shear production term, $-\langle u'v' \rangle (\partial \langle u \rangle / \partial y)$, due to the decrease of the turbulent shear stress, $\langle u'v' \rangle$. In the budget of $\langle u'u' \rangle$ for the rotating channel, the reduction of $\langle u'u' \rangle$ due to the decrease of the shear production term was more significant than the reduction due to the Coriolis force term.

The diagram for the turbulence suppression observed in the present study can be summarized as follows. A large truncation error due to the rotational form in the y-momentum equation primarily reduces the turbulent shear stress and the fluctuations normal to the wall, acting similarly to the Coriolis force term. In turn, it dampens the shear production term for the streamwise component of fluctuations, and subsequently, the streamwise fluctuation is suppressed.

We note that, corresponding to the nonconservation of the turbulent kinetic energy in the extra term due to the truncation error, kinetic energy is not conserved in the discretized sense when the rotational form is used.

4.3. *DNS of Rotating Channel Flow*

For comparison, we carried out DNS of rotating channel flow, in which the Coriolis force with an angular velocity of Ω_R with $C_R = -0.0115$ about the z-axis was explicitly applied as

$$\frac{\partial u_i}{\partial t} + \frac{\partial (u_i u_j)}{\partial x_j} = -\frac{\partial p^*}{\partial x_i} + \frac{1}{\mathrm{Re}} \frac{\partial^2 u_i}{\partial x_k \partial x_k} - 2\epsilon_{imn} \Omega_m u_n - \delta_{i2} \frac{r^2}{2} \frac{\partial \Omega_R^2}{\partial x_i}, \tag{27}$$

where $(\Omega_1, \Omega_2, \Omega_3) = (0, 0, \Omega_R)$, ϵ_{ijk} is the alternating tensor, and p^* is the reduced static pressure:

$$p^* = p - \frac{1}{2} \Omega_R^2 r^2. \tag{28}$$

The term, $\frac{1}{2}\Omega_R^2 r^2$, is the centrifugal force potential caused by system rotation, where r is the distance of any point in the field from the axis of rotation. The skew-symmetric form was used for the convective terms throughout the channel in conjunction with the second-order finite differences (Eq. (7)) for first-order partial differential operators in the y direction (Case III).

Because of the dependence in Ω_R on the y-coordinate and the nonintegrability of the term, Ω_R^2 with respect to y, the last term in Eq. (27) was not absorbed into the centrifugal force potential, unlike in the pure rotating channel.

The last term in Eq. (27) yields the extra term in the budget of the Reynolds shear stress, $\langle u'v' \rangle$, given as

$$\left\langle \frac{u' r^2}{2} \frac{\partial \Omega_R^2}{\partial x_i} \right\rangle = \frac{1}{2} \langle u' r^2 \rangle \frac{\partial \Omega_R^2}{\partial x_i}. \tag{29}$$

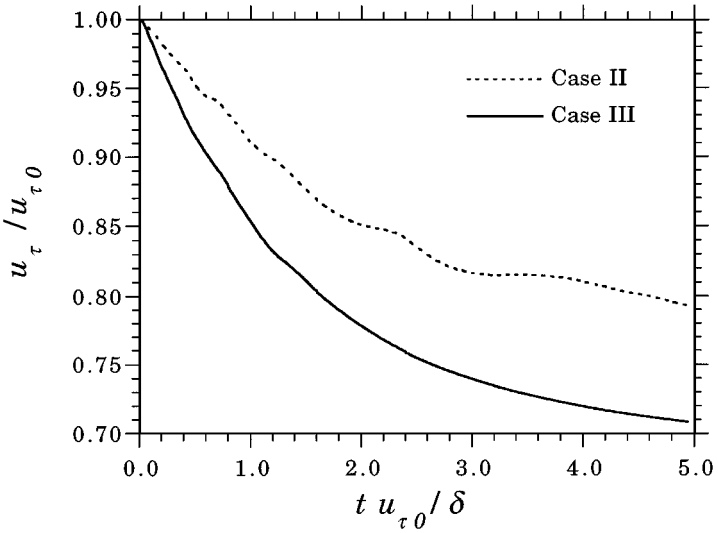

FIG. 13. Time evolution of the wall friction velocity, u_τ, at the lower wall obtained for Case II and Case III.

Since the term r^2 is deterministic, $\langle u' r^2 \rangle = \langle u' \rangle \langle r^2 \rangle = 0$, this extra term is negligible in the budget of the Reynolds shear stress on average, although the computed value of this term may not be exactly equal to zero because of the finite statistical sample size used in computing averages. A similar extra term is yielded in the budget of $\langle v'v' \rangle$, but the contribution of this term is also negligible on average.

Figure 13 shows the time development of the wall friction velocity at the lower wall obtained from Case III. Similar results were obtained at the upper wall (figure not shown). Its temporal variation is qualitatively similar to the development of u_τ, obtained using the rotational form obtained for Case II, but u_τ, obtained for Case III, decreases rapidly. We consider that this difference is attributable to the difference between the rotational stress generation term and the truncation error term in the budget of $\langle v'v' \rangle$ shown in Fig. 12. The amplitude of the truncation error term is smaller than that of the rotational stress generation term, which is consistent with the slower decay of turbulence in the result obtained using the rotational form in Case II. This slower decay may also be attributable to the absence of the truncation error term in the budget of $\langle u'u' \rangle$.

5. ELIMINATION OF LARGE TRUNCATION ERRORS

Large truncation errors found in the previous section were generated because the product rule [10],

$$\frac{\partial (fg)}{\partial y} = \frac{\partial f}{\partial y} g + f \frac{\partial g}{\partial y}, \tag{30}$$

is not satisfied when the conventional finite difference scheme is used for the first-order partial differential operator $\partial / \partial y$. This inaccuracy in approximating the product rule is significant when the first- and second-order finite differences (Eqs. (6) and (7)) are used. We have found that, when the third- or fourth-order finite differences are used, the inaccuracy of the approximation of the product rule is substantially reduced, and the laminarization of

the turbulent state observed in Section 3 is prevented (data not shown). The drawback of the higher-order finite differences is that the additional boundary conditions are required near the walls.

A scheme which satisfies the product rule, even when the second-order finite differences are used, was considered by Schumann [19]. Recent works by Kajishima [20, 21], Suzuki and Kawamura [22], and Kawamura and Kondoh [23] showed that, when the term $\left(f(\partial g/\partial y)\right)_j$ is approximated as

$$\left(f\frac{\partial g}{\partial y}\right)_j \sim \alpha\frac{f_{j+1}+f_j}{2}\frac{g_{j+1}-g_j}{h_{j+1}} + (1-\alpha)\frac{f_j+f_{j-1}}{2}\frac{g_j-g_{j-1}}{h_j}, \tag{31}$$

the product rule is satisfied because the terms on the right-hand side of Eq. (31) can be rewritten as

$$\begin{aligned}&\left\{\alpha\frac{f_{j+1}g_{j+1}-f_jg_j}{h_{j+1}} + (1-\alpha)\frac{f_jg_j-f_{j-1}g_{j-1}}{h_j}\right\}\\ &\quad-\left\{\alpha\frac{g_{j+1}+g_j}{2}\frac{f_{j+1}-f_j}{h_{j+1}} + (1-\alpha)\frac{g_j+g_{j-1}}{2}\frac{f_j-f_{j-1}}{h_j}\right\}\\ &\quad\sim\left\{\frac{\partial(fg)}{\partial y}\right\}_j - \left(g\frac{\partial f}{\partial y}\right)_j,\end{aligned}$$

where α is arbitrary, in order to satisfy the product rule, but it is generally chosen to be equal to $h_j/(h_{j+1}+h_j)$. Therefore, this scheme is consistent with the product rule (referred to as the consistent scheme [22] below). In the consistent scheme, the convective terms formulated by the skew-symmetric, divergence, and convective forms are algebraically equivalent to each other so long as the continuity equation of the velocity field is ensured. These second-order-accuracy consistent schemes can be extended to the fourth-order-accuracy schemes [20, 21].

When the rotational form is used in conjunction with the consistent scheme, a large truncation error presented in the previous section can be eliminated, because in this scheme,

$$\frac{\delta u^2}{\delta y} = 2u\frac{\delta u}{\delta y}. \tag{32}$$

It should be noted, however, that another drawback of the rotational form, i.e., the occurrence of large aliasing errors, is not eliminated, even when the consistent scheme is used. Therefore, when dealiasing is not performed for the convective terms, we consider that the skew-symmetric form, used in conjunction with the consistent scheme, still yields better results, because the aliasing errors are reduced in the skew-symmetric form [9].

An alternative scheme which eliminates the large truncation error is the one used by Kravchenko and Moin [10]. They conducted LES of turbulent channel flow using the dealiased Fourier pseudospectral method in the x and z directions, and the B-spline method in the wall-normal direction. The streamwise component of the velocity u was expanded as

$$u(x,y,z,t) = \sum_{k_x,j,k_z}\tilde{u}_j(k_x,k_z,t)\,e^{ik_xx}e^{ik_zz}B_j^k(y), \tag{33}$$

where $B_j^k(y)$ is the B-spline of order k, and k_x and k_z denote the wave numbers, respectively, in the x and z directions. $B_j^k(y)$ is defined on a set of knot points t_j [10]. In this method,

the term $(u(\partial u/\partial y))$ is evaluated via the discrete weak form as

$$\int_V e^{-ik_x x} e^{-ik_z z} B_l^k(y) \left(u \frac{\partial u}{\partial y} \right) dx\, dy\, dz \tag{34}$$

$$= \sum_m \sum_n \left[\int B_l^k(y) \left\{ B_m^k(y) \frac{\partial B_n^k(y)}{\partial y} \right\} dy \right] \tilde{u}_m \tilde{u}_n, \tag{35}$$

using the method of weighted residuals, where V denotes the entire computational domain. Similarly, the term $\partial u^2/\partial y$ can be evaluated as

$$\sum_m \sum_n \left[\int B_l^k(y) \frac{\partial}{\partial y} \{ B_m^k(y) B_n^k(y) \}\, dy \right] \tilde{u}_m \tilde{u}_n. \tag{36}$$

Because $B_j^k(y)$ are the (piecewise) polynomials, Eq. (36) can be rewritten as

$$\begin{aligned} &\sum_m \sum_n \left[\int B_l^k(y) \left\{ B_m^k(y) \frac{\partial B_n^k(y)}{\partial y} \right\} dy \right] \tilde{u}_m \tilde{u}_n \\ &\quad + \sum_m \sum_n \left[\int B_l^k(y) \left\{ B_n^k(y) \frac{\partial B_m^k(y)}{\partial y} \right\} dy \right] \tilde{u}_m \tilde{u}_n \end{aligned} \tag{37}$$

$$= 2 \sum_m \sum_n \left[\int B_l^k(y) \left\{ B_m^k(y) \frac{\partial B_n^k(y)}{\partial y} \right\} dy \right] \tilde{u}_m \tilde{u}_n. \tag{38}$$

Therefore, in this method, Eq. (32) is satisfied and the large truncation error does not arise, even when the rotational form is used.

In summary, the integration-by-parts used analytically in derivations of conservation properties can also be directly applied to some discretization methods, namely, the consistent scheme and the Kravchenko–Moin scheme.

6. CONCLUSIONS

The truncation error of the rotational form for the convective terms in the Navier–Stokes equation is examined. The flow field which was considered in the present study, was the fully developed turbulent channel flow. The direct numerical simulation (DNS) method was used to solve the Navier–Stokes and continuity equations. The partial derivatives in the wall-normal direction were approximated by the first- and second-order finite difference method.

It was shown that the major error comes from the truncation error in the normal component of the momentum equation. The heuristic estimate of the truncation error using the Taylor expansion revealed that this truncation error term is comparable to the difference between the streamwise and normal components of the turbulence fluctuations represented by the nonlinear $k - \epsilon$ model in the Reynolds averaged turbulence models. Therefore, in the governing equations for the Reynolds shear stress and the normal stress, this truncation error term behaves analogously to the rotational stress generation term due to the Coriolis force acting in the channel flow rotating about the spanwise axis.

Similarities to and differences from the conventional rotating channel flow were discussed. The effective angular velocity due to the truncation error term was dependent on

the distance from the wall, and the turbulence was reduced on both sides of the walls. The results were in good agreement with the previous results obtained using the large-eddy simulation method [7].

The DNS of the channel flow rotating with this effective angular velocity was further conducted to assess this analogy. The time development of the wall friction velocity was similar to that obtained in DNS using the rotational form.

Numerical schemes which eliminate the large truncation error for the rotational form were discussed.

The truncation errors are roughly divided into two groups: dissipative errors and dispersive errors. When the convective terms are approximated using the central finite differences, the Taylor expansion of the truncation error shows that the error term is generally dispersive [24]. In fact, when the estimates of the truncation errors, Eq. (11) and Eq. (12), are integrated with respect to y from the lower wall to the upper wall, the integrals vanish; i.e., the momentum is neither increased nor decreased by the truncation error term. The decay of turbulence previously observed in the numerical simulation was mostly attributable to the excessively dissipative errors [24]. In the present study, we have shown that some dispersive error can also induce the decay of turbulence due to the nonlinearity of the convective terms. Some care should be taken in dealing with the low-order finite difference method, because the truncation error terms of the multiples of the $\partial u/\partial y$ term, usually associated with the first- or second-order finite difference method, can lead to erroneous results particularly in turbulent flows with strong shear.

ACKNOWLEDGMENTS

This paper is dedicated to the late Prof. Kunio Hijikata (Tokyo Institute of Technology). This work was partially supported by a Grant-in-Aid from the Ministry of Education, Science, Sports and Culture, Japan (No. 07650190), and the Project for Parallel Processing and Supercomputing at the Computer Centre, University of Tokyo.

REFERENCES

1. N. A. Phillips, An example of nonlinear computational instability, in *The Atmosphere and Sea in Motion* (Rockefeller Inst., New York, 1959), p. 501.
2. A. Arakawa, Computational design for long-term integration of the equations of fluid motion: two-dimensional incompressible flow, Part I, *J. Comput. Phys.* **1**, 119 (1966).
3. D. Kwak, *Three-Dimensional Time Dependent Computations of Turbulent Flow*, Ph.D. thesis, Department of Mechanical Engineering, Stanford University, 1975.
4. D. O. Gottlieb and S. A. Orszag, *Numerical Analysis of Spectral Methods: Theory and Applications*, NSF-CBMS Monograph, Vol. 26 (Soc. Indus. Appl. Math., Philadelphia, PA, 1977).
5. N. N. Mansour, *Large-Eddy Simulation of a Turbulent Mixing Layer*, Ph.D. dissertation, Stanford University, 1978.
6. P. Moin and J. Kim, Numerical investigation of turbulent channel flow, *J. Fluid Mech.* **118**, 341 (1982).
7. K. Horiuti, Comparison of conservative and rotational forms in large eddy simulation of turbulent channel flow. *J. Comput. Phys.* **71**, 343 (1987).
8. T. A. Zang, On the rotation and skew-symmetric forms for incompressible flow simulations, *Appl. Numer. Math.* **7**, 27 (1991).
9. G. A. Blaisdell, E. T. Spyropoulos, and J. H. Qin, The effect of the formulation of nonlinear terms on aliasing errors in spectral methods, *Appl. Numer. Math.* **20**, 1 (1996).
10. A. G. Kravchenko and P. Moin, On the effect of numerical errors in large eddy simulations of turbulent flows, *J. Comput. Phys.* **131**, 310 (1997).

11. K. Horiuti, A proper velocity scale for modeling subgrid-scale eddy viscosity in large eddy simulation, *Phys. Fluids A* **5**, 146 (1993).
12. J. Kim, P. Moin, and R. Moser, Turbulence statistics in fully developed channel flow at low Reynolds number, *J. Fluid Mech.* **177**, 133 (1987).
13. J. Jimenez and P. Moin, The minimal flow unit in near-wall turbulence, *J. Fluid Mech.* **225**, 213 (1991).
14. M. Nishioka, S. Furumoto, T. Ozaki, and M. Asai, Characteristics of turbulent boundary layer at low Reynolds numbers, in *Proc. 25th Turbulence Symposium, Japan Society of Fluid Mechanics, Sendai, July 1993*, p. 30. [Japanese]
15. R. D. Moser and P. Moin, The effect of curvature in wall-bounded turbulent flows, *J. Fluid Mech.* **175**, 479 (1987).
16. C. G. Speziale, Analytical methods for the development of Reynolds-stress closures in turbulence, *Annu. Rev. Fluid Mech.* **23**, 107 (1991).
17. K. Horiuti, Higher-order terms in the anisotropic representation of Reynolds stresses, *Phys. Fluids A* **2**, 1708 (1990).
18. J. P. Johnston, R. M. Halleen, and D. K. Lezius, Effects of spanwise rotation on the structure of two-dimensional fully developed turbulent channel flow, *J. Fluid Mech.* **56**, 533 (1972).
19. U. Schumann, Subgrid scale model for finite difference simulations of turbulent flows in plane channels and annuli, *J. Comput. Phys.* **18**, 376 (1975).
20. T. Kajishima, A higher order finite difference method for wall bounded incompressible flows, in *Proc. 5th Int. Symp. Comput. Fluid Dyn., Vol. I, 1993*, p. 414.
21. T. Kajishima, Conservation properties of finite difference method for convection, *Trans. JSME* Ser. B **60**(574), 2058 (1994). [Japanese]
22. T. Suzuki and H. Kawamura, Consistency of finite-difference scheme in direct numerical simulation of turbulence, *Trans. JSME* Ser. B **60**(578), 58 (1994). [Japanese]
23. H. Kawamura and Y. Kondoh, Application of consistent finite difference scheme to DNS of turbulent heat transfer in channel flow, in *Proc. 3rd KSME-JSME Thermal Engineering Conference, Kyongju, Korea, Oct. 1996*, p. I-53.
24. E. S. Oran and J. P. Boris, *Numerical Simulation of Reactive Flow* (Elsevier Science, New York, 1987).